ELSEVIER

Computers and Electronics in Agriculture
34 (2002) 25–42

Computers and electronics in agriculture

www.elsevier.com/locate/compag

# Numerical and experimental study of airflow in a typical refrigerated truck configuration loaded with pallets

J. Moureh *, N. Menia, D. Flick

*Refrigerating Process Engineering Research Unit, Cemagref, BP 44, 92163 Antony cedex, France*

**Abstract**

This work is part of a research activity aiming to improve and to optimize air-distribution systems in refrigerated vehicles in order to decrease the temperature differences within the load. The present study reports on the numerical and experimental characterization of airflow generated within a semi-trailer enclosure loaded with pallets. In the studied configuration, inlet and outlet sections were placed in the front of the trailer. This is a very common configuration and is extensively used in refrigerated transport. The experiments were carried out on a reduced-scale model built with a ratio 1/3.3 of a trailer. The numerical modeling of airflow was performed using the computational fluid dynamics (CFD) code Fluent and two levels of turbulence modeling: the standard $k-\varepsilon$ model and a model with a second-moment closure, the Reynolds stress model (RSM). Only the results obtained using the RSM model showed agreement with the experimental data. 

*Keywords:* Airflow; Refrigerated vehicle; Laser–Doppler velocimetry; Ventilation; Numerical modeling; Computational fluid dynamics

## Nomenclature

$C_\mu$ turbulence model coefficient
$D_H$ hydraulic diameter of the inlet section
$I$ turbulence intensity (%)

* Corresponding author.

0168-1699/02/$ - see front matter 
PII: S0168-1699(01)00178-8

$K_p$ permeability coefficient ($m^2$)
$k$ kinetic energy of turbulence ($m^2/s^2$)
$p$ static pressure (Pa)
$Q$ flow rate ($m^3/s$)
$Re$ Reynolds number
$U_i$, $u_i$ mean, fluctuating velocity component in $x_i$ direction (m/s)
$x$, $y$, $z$ lateral, vertical and longitudinal coordinates (m)

*Greek symbols*
$\rho$ density ($kg/m^3$)
$\nu$ kinematic viscosity ($m^2/s$)
$\mu$ viscosity (kg/m s)
$\varepsilon$ turbulence energy dissipation rate ($m^2/s^3$)

*Subscripts*
0 inlet
m maximum
t turbulent
$i$, $j$, $k$ vector directions

## 1. Introduction

In refrigerated transport, maintaining regular temperature throughout the cargo is essential to preserve quality, safety and shelf life of perishable foods. In the refrigerated enclosure, the control of temperature and temperature homogeneity is directly governed by airflow patterns. Air renewal provided by these airflows should compensate for the overall heat fluxes exchanged locally through the insulated walls or generated by the products. This process is essential in order to decrease temperature differences throughout the cargo.

In the refrigerated vehicle enclosure (RVE), the air is supplied at relatively high velocities through a small inlet section located adjacent to or near the ceiling. From an aerodynamic perspective, the principal feature of the RVE configuration is the presence of inlet and exit sections of airflow on the same surface located at the front of the vehicle. In addition to this asymmetrical airflow design, the compactness of the cargo and high resistance to airflow due to thin air spaces between pallets result in uneven air distribution in the cargo. Consequently, stagnant zones with poor ventilation can be found, especially in the rear part of the vehicle. In these zones, higher temperatures can occur locally within the load (Lenker et al., 1985; Gögus and Yavuzkurt, 1974; LeBlanc et al., 1994; Bennahmias and Labonne, 1993;

Meffert and Van Nieuwenhuizen, 1973) even though the refrigerating capacity is higher than heat fluxes exchanged by the walls and the products (Billiard et al., 1990).

The objective of this study was to investigate numerically and experimentally the airflow pattern throughout a vehicle enclosure loaded with two rows of pallets. The developed model was investigated using the computational fluid dynamics (CFD) code Fluent and two levels of turbulence modeling were used and compared. The Reynolds stress model (RSM) based on the second-moment closure as described by Launder et al. (1975) and the standard $k-\varepsilon$ model (Launder and Spalding, 1974) were assessed. To validate the model, predicted values of velocity and airflow patterns were compared with experimental data obtained on a scale model under isothermal conditions. After adequate validation, the model could used as a design tool to optimize more complex configurations, reducing the need for expensive and time-consuming experiments.

## 2. Bibliographical analysis

Recent investigation showed that little or no research on the characterization of air velocities in a truck loaded with pallets has been performed. This can be attributed to the complexity of direct measurement of local air velocities and flow rates in the thin air spaces located between pallets and boxes. However, an experimental approach used by Lindqvist (1998, 1999) to measure pressure inside a full-scale laboratory model of reefer hold loaded with pallets showed very poor distribution of airflow within the vessel. The same study also showed that high pressure gradients reflecting high velocities were located in the front of the vessel, and in contrast, weak pressure gradients/or velocities were present at the rear of the vessel.

Several modeling approaches using electrical analogies to predict the airflow rate in spacings or channels between pallets or boxes were developed by Wang and Touber (1988), Meffert and Van Beek (1983), Ménia et al. (2002). These approaches could give qualitative information on the air circulation rate and do not require much time or memory capacity. However, these simplified modeling approaches were not able to provide quantitative predictions of airflow patterns, local air velocities and turbulence levels which are important in heat transfer phenomena. In addition, predictions can not take into account the behavior, the stability and the diffusion of the supplied forced air jet.

Numerical predictions of air velocities and temperature distributions can be obtained by solving sets of differential equations of mass, momentum and energy written in their conservative form using the finite-volume method. Using CFD codes, computers and processing facilities, complex configurations such as refrigerated transport or storage have been studied by many authors (Ménia et al., 2002; Wang and Touber, 1990; Van Gerwen and Van Oort, 1989; Hoang et al., 2000).

Wang and Touber (1990) used the CFD code Phoenics and the $k-\varepsilon$ model to predict airflow, temperature and moisture patterns, in a refrigerated room. Numer-

ical resolution was performed on the assumption that forced convection dominated the heat transfer. Validation was performed on the basis of temperature evolution. Because the air velocities were not measured, the validation and the reliability of the model cannot be confirmed.

Van Gerwen and Van Oort (1989) also used the Phoenics CFD package to predict air velocities and product temperature based on cooler airflow rate, product properties and the geometry of cold store and storage pattern. In this model, the authors gave design recommendations in order to better homogenize airflow circulation and temperature levels in the load. However, no data were given by the authors concerning the numerical approach, the turbulence model, the boundary conditions, the experimental and numerical data, the validation procedure and its accuracy. Consequently, such models are difficult to evaluate.

More recently, Hoang et al. (2000) used the CFX CFD package code to predict the airflow pattern in empty and loaded cold stores. The forced-circulation air cooler unit was modeled using an appropriate body force and resistance, corresponding to the characteristics of the fan and the tube bank-evaporator. Validation was performed by comparisons of numerical and experimental data on vertical profiles of air velocity magnitudes. The accuracy was 26% for the standard $k-\varepsilon$ model and 28.5% for the RNG model. According to the authors, the Coanda effect governing the attachment of the jet on the ceiling was not well predicted by the $k-\varepsilon$ model. Moreover, validation of this model lacks comparisons between numerical and experimental data regarding such aspects as airflow patterns, diffusion of the jet leaving the cooler and turbulence profiles.

Many studies use the $k-\varepsilon$ model since it is easy to programme and has good stability and broad applicability. However, predictions given by this model are often not accurate and modifications are performed to improve the computed results, especially in empty slot-ventilated enclosures where experimental data are easier to obtain. To improve numerical predictions, Choi et al. (1990) suggested modifying the multiplicator coefficient $C_\mu = 0.09$ of the turbulent viscosity given by the standard $k-\varepsilon$ model. In a comparison of different $k-\varepsilon$ models for indoor airflow, Chen (1995) showed that all these models studied were unable to predict the presence of the secondary recirculating flow. These bad predictions given by the $k-\varepsilon$ model can be attributed to the complexity of the airflow in a room since it is often the combination of free turbulent shear flows, near wall effect, pressure gradient implying the presence of separating and reattaching jet, primary and secondary recirculating including high streamline curvature effect (Chen, 1995; Choi et al., 1990; Awbi, 1989; Davidson, 1989; Nielsen et al., 1978; Hoff et al., 1992). In addition, a more complicated and complex system can be expected due to the presence of the load. For such complex flows, fundamental studies (Wilcox, 1994; Menter, 1997; Nallasamy, 1987) agree on the inadequacy of the $k-\varepsilon$ model and underline its limitations by comparison with experimental data. In this case, improving predictions can be achieved by taking into account the effect of the turbulence anisotropy by using models based on the second-moment closure.

## 3. Experimental device

The experiments were carried out on a scale model of a slot ventilated enclosure built with a ratio 1:3.3 of a trailer with respect to the adimensional Reynolds number. All the data, dimensions, flow rate and the results were expressed according to the actual scale (Fig. 1). The walls of the scale model were composed of wood. The front wall was constructed of glass to make airflow measurements

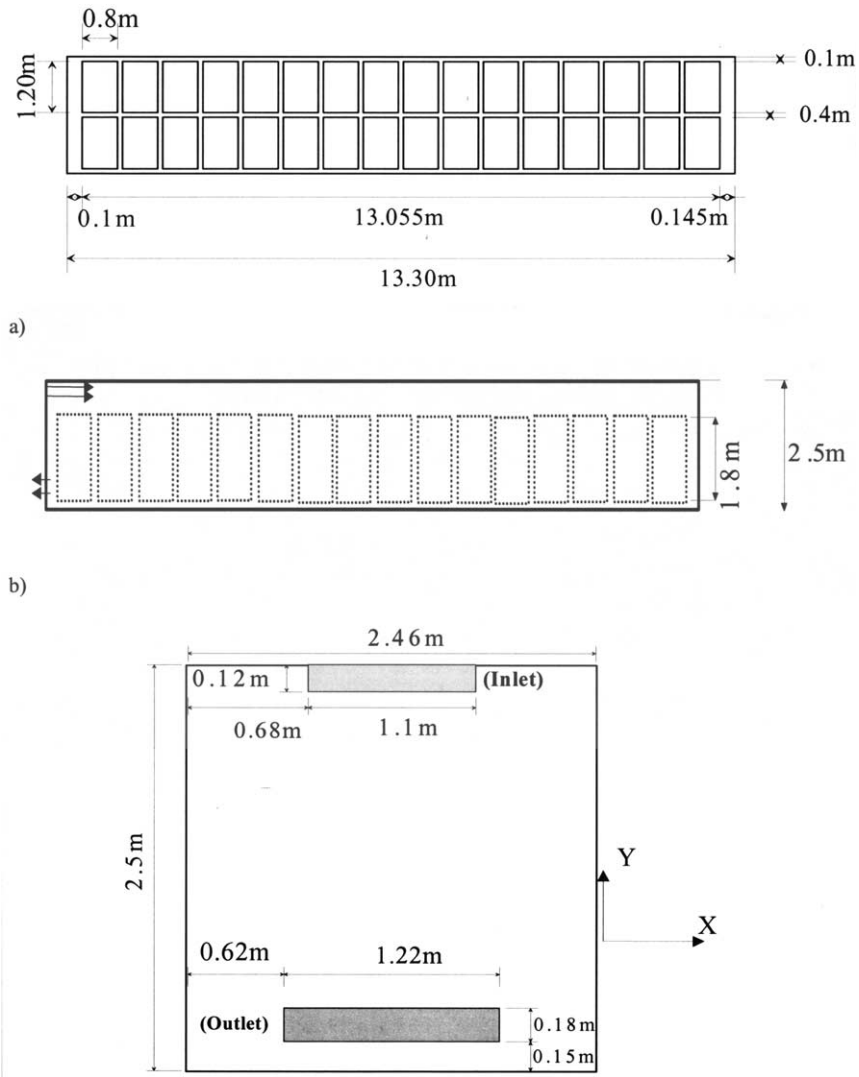


Fig. 1. Dimensions of studied vehicle configuration. (a) Top view of cargo. (b) Side view of the load. (c) Cross-view section of the front face of the vehicle.

using Laser–Doppler velocimetry easier to perform. The inlet and outlet sections are located on the same surface at the front of the trailer. Inside the scale model, closed glass boxes are used to represent pallets.

The mean velocity and its fluctuations were obtained with a one-dimensional Laser–Doppler anemometer placed outside the model in order to avoid interference with the flow. The anemometer comprised a 50 mW laser diode emitting a visible red beam at 690 nm wavelength, a beamsplitter, a Brag cell, a focussing and receiving lens and pinhole arrangement to collect scattered light from the measurement value and a photomultiplier. Light scattered from particles was captured through the same front lens from which the two beams exit. The air supplied to the model room passed through atomizers and allowed near continuous Doppler signals, which were converted to velocity and time. The system was able to correctly determine the sign as well as the magnitude of the velocity component.

## 4. Numerical modeling approach

### *4.1. Porous medium concept based on Darcy's law*

As there was a big difference between pallet dimensions and the thin air spacings located between them (Fig. 1), the grid size will exceed the memory capacity and the computing time will be excessive especially if we want to apply a gradual grid refinement where the size ratio between two consecutive cells should not exceed approximately 20%.

To avoid this difficulty, we replaced thin air spaces between pallets along the vehicle by a fictitious, aerodynamically equivalent porous medium for which the permeability coefficient was chosen so as to ensure the same airflow resistance as the actual medium. This approach was made possible because air velocity measurements showed that laminar flow was dominant between pallets ($Re < 500$). Consequently, there is a relationship between the airflow rate and pressure gradient as in a porous medium governed by Darcy's law.

In the proposed system, the permeability coefficient for a porous medium was chosen in order to ensure that for a given pressure gradient, the same flow rate for the actual medium exists. Consequently, the analogy between the laminar flow between two parallel plates separated by a distance $e$ and a flow in a porous medium between two parallel plates separated by a distance $e'$ are related as follows:

$$(V_{\text{mean}}e)_{\text{actual medium}} = (V_{\text{mean}}e')_{\text{porous medium}} \Rightarrow \left(\frac{\mathrm{d}p}{\mathrm{d}x}\frac{e^2}{12\mu}\right)e = \left(-\frac{K_{\text{p}}}{\mu}\frac{\mathrm{d}p}{\mathrm{d}x}\right)e' \quad (1)$$

The equivalent permeability is equal to:

$$K_{\text{p}} = \frac{e^3}{12e'} \quad (2)$$

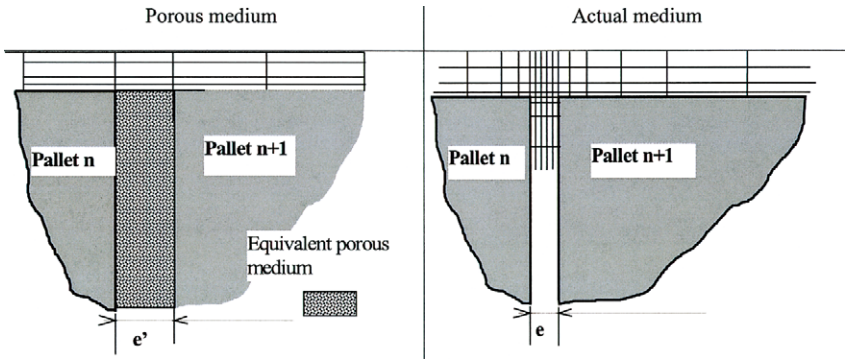


Fig. 2. Analogy between laminar and porous medium on the grid refinement.

The use of this analogy allows the reduction in grid size because air spaces separating pallets to be represented by a single porous cell with a permeability coefficient that was calculated from Eq. (2). In addition, this cell can be bigger than the real pallet spacing ($e'/e = 4$ for example). Fig. 2 illustrates the effect of this analogy on grid refinement and consequently on grid size.

### 4.2. Governing equations and hypothesis

The time-averaged Navier–Stokes differential equations for steady, high-Reynolds numbers and incompressible flows are expressed in their conservative form using Cartesian coordinates as follows:

Mass conservation:

$$\frac{\partial U_j}{\partial x_j} = 0 \tag{3}$$

Momentum conservation:

$$\frac{\partial U_j U_i}{\partial x_j} = -\frac{1}{\rho}\frac{\partial P}{\partial x_i} + \frac{\partial}{\partial x_i}\left(v\frac{\partial U_i}{\partial x_j} - \overline{u_i u_j}\right) \tag{4}$$

The Reynolds turbulent stress $\overline{u_i u_j}$ depends on the turbulence closure. In the situation investigated, two levels of turbulence modeling closure have been employed.

Firstly, using the standard $k-\varepsilon$ model based on the Boussinesq hypothesis (Launder and Spalding, 1974);

$$-\overline{u_i u_j} = v_i\left(\frac{\partial U_i}{\partial x_j} + \frac{\partial U_j}{\partial x_i}\right) - \frac{2}{3}k\delta_{ij} \tag{5}$$

the eddy (turbulent) viscosity $v_t$ is obtained from:

$$v_t = C_\mu \frac{k^2}{\varepsilon} \tag{6}$$

Secondly, using a second-moment closure with the RSM (Launder et al., 1975).

The $k$–$\varepsilon$ model uses the turbulent viscosity in the time–mean momentum equations. This model has been applied with good accuracy to various situations involving air movement since it is easy to programme, has good stability and broad applicability. However, in some complex flows particularly involving boundary layer separation or reattachment, the shear stress may be absent where the mean velocity gradient is not equal to zero and vice versa. Such flows cannot be predicted by the Boussinesq turbulent viscosity concept because in reality, the turbulent stresses are not directly related to the mean velocity gradient. This can explain the use of more advanced turbulence models such as the RSM, for which an individual transport equation is derived for each shear stress component.

### *4.3. Boundary conditions*

The computational domain may be surrounded by inflow and outflow boundaries in addition to symmetry and solid walls. At the inlet, uniform distribution was assumed for velocity components, kinetic energy of turbulence $k_0$ and the energy dissipation rate $\varepsilon_0$. The numerical values are specified as:

- $(U_{0x} = U_{0y} = 0$; $U_{0z} = U_0 = 11.5$ m/s representing the mean longitudinal velocity, giving an inlet flow rate $Q_0 = 5500$ m$^3$/h;
- $k_0 = 3/2\ (U_0 I_{0z})^2$; where $I_{0z} \approx 10\%$ represents the measured turbulence intensity of the $z$-component of velocity at the inlet;
- $\varepsilon_0 = (C_\mu^{0.75} k_0^{1.5}/0.07\ D_H)$ where $D_H$ represents the hydraulic diameter of the inlet section;
- for the RSM model, turbulence was assumed to be isotropic:

$$\overline{u_i u_j} = \frac{2}{3} k_0 \delta_{ij}.$$

At the outflow, pressure was considered to be uniform and a zero-gradient condition was applied for all transport variables.

The turbulence models were only valid in fully turbulent regions. Close to the wall, where viscous effects become dominant, the model was used in conjunction with wall functions. For this study, the conventional equilibrium logarithmic law governing the wall was used (Launder and Spalding, 1974).

For the symmetry plane, zero normal velocity and zero normal gradients of all variables were applied.

The computations were carried out using the CFD code Fluent, on a three-dimensional configuration. The governing equations were solved using the finite-volume method in a staggered grid system. Non-uniform grid distribution was used in this study, with finer grid in regions near the inlet, outlet and walls where high gradients were expected.

In this study the grid selected for the results presented below was very fine, with $50 \times 52 \times 240$ grid cells representing half depth (1.23 m) $\times$ height (2.5 m) $\times$ length

(13.3 m), which was equal to 624 000 cells for the empty configuration and 419 000 cells for the loaded configuration as the load is not part of the modeled domain. The computation time was approximately 3 days. It was conducted on a personal computer equipped with a 450 MHz processor.

However, a lot of simulations made with coarser grids, not presented here, show for greater than 350 000 cells the predicted values are grid-independent.

## 5. Results and discussion

### 5.1. Airflow pattern behavior

Fig. 3 presents a comparison between loaded and empty enclosures showing the behavior of the streamlines on the symmetry plane. In the case of the unloaded configuration, numerical results obtained by the RSM model agree very well with experimental data (Fig. 3a) which were obtained from 1080 ($24 \times 45$) measurement points made by the LDV system. Fig. 4 presents a comparison of experimental and numerical data concerning the decrease in velocity from the inlet section (center of trailer) in a loaded configuration. These figures show clearly that the wall jet separates from the ceiling at approximately 10 m in the case of an empty enclosure and 5 m in the loaded configuration. This separation splits the jet into two regions dominated by two vortices of opposite circulation. The primary recirculation located on the front part of the enclosure restricts the range and the action of the inlet jet. Conversely, the secondary flow located in the rear part is weakly supplied by the primary jet. Hence, the velocities are very low ($V \leq 0.2$ m/s) in this section.

After leaving the inlet and due to the Coanda effect, the jet attaches to the ceiling. However, the separation of the jet from the wall over a certain distance from the inlet needs analysis of the external flow generated by the outlet and its impact on the blowing jet. The reverse flow of the outlet implies the formation of a positive pressure gradient ($\mathrm{d}p/\mathrm{d}z > 0$; $z$ is oriented towards the rear). This gradient was favorable to the reverse flow and unfavorable to the inlet wall jet. Fig. 5 presents the evolution of the static pressure through the inlet section along the enclosure in the loaded configuration. This evolution indicated the presence of a high positive (adverse) pressure gradient at the end of the primary recirculating area where the separation of the jet from the wall occurs. After this separation, the pressure gradient is very low, causing low air velocities in the secondary recirculating area.

### 5.2. Performance of the turbulence modeling

Figs. 3 and 4 clearly show the ability of the RSM model to simulate the secondary recirculation and to correctly predict the general behavior of air movement related to the primary and to the second recirculations in loaded and unloaded configurations.

In the case of the loaded configuration, the RSM and the $k-\varepsilon$ models predicted the separation of the jet from the wall. However, the RSM model predicted the separation of the jet from the wall at approximately 5 m in accordance with experimental data while the $k-\varepsilon$ model predicted this separation at 8 m.

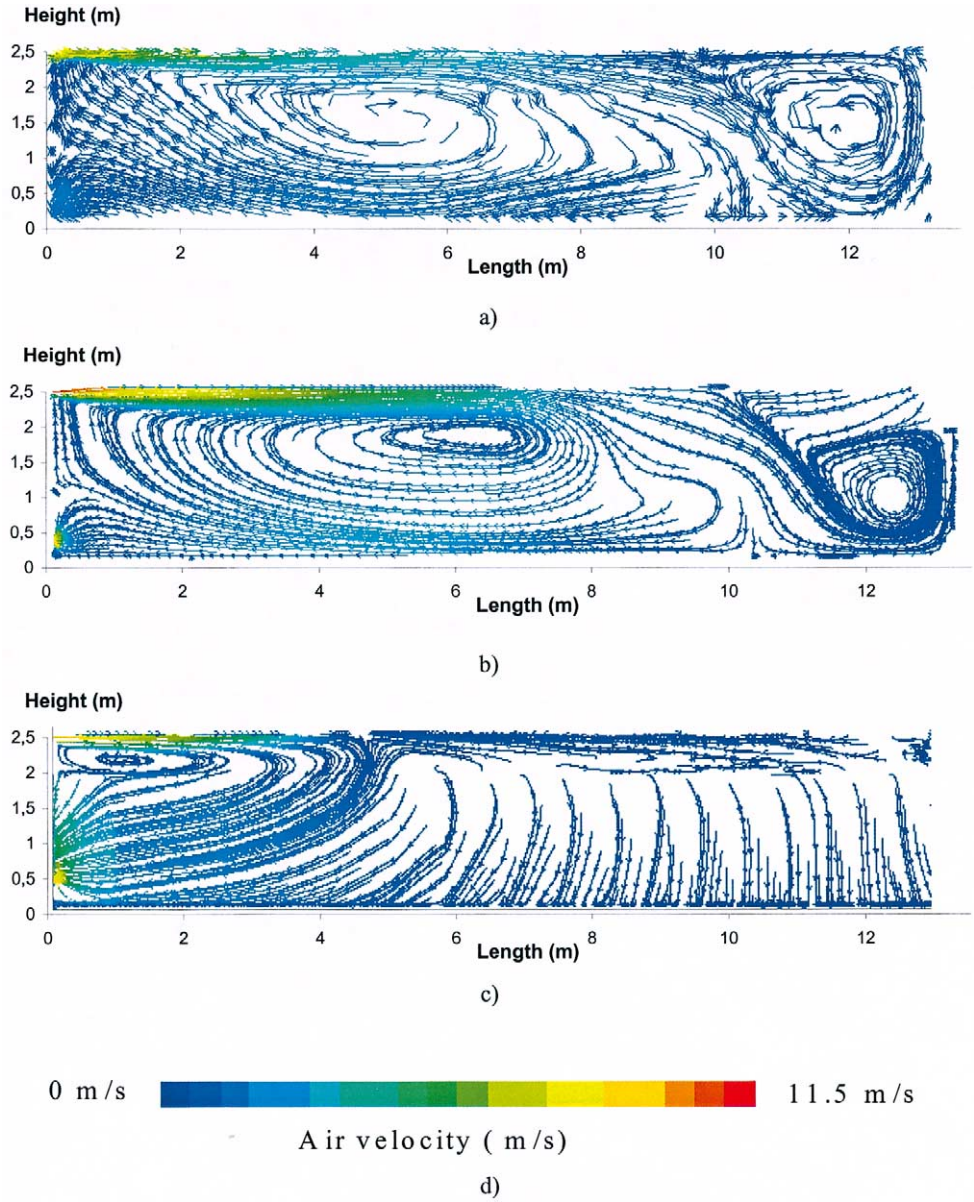


Fig. 3. Influence of the load on the airflow pattern. (a) Streamlines in unloaded configuration, Laser–Doppler measurements (1100 points). (b) Streamlines in unloaded configuration, RSM model. (c) Streamlines in loaded configuration, RSM model. (d) Air velocity scale.

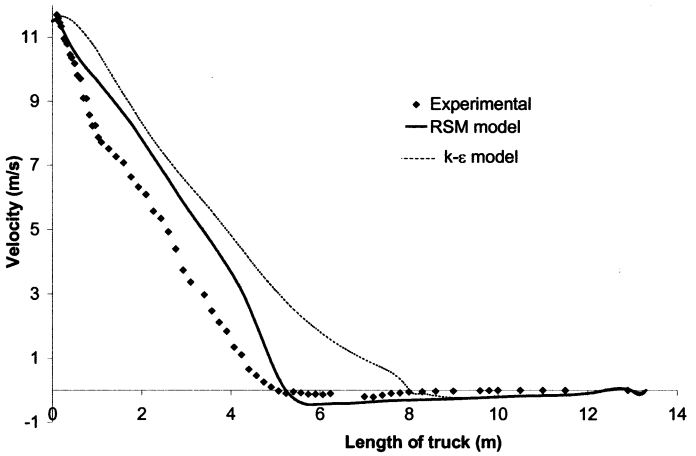


Fig. 4. Evolution of the jet velocity along the trailer.

For the unloaded configuration, the $k-\varepsilon$ model failed to predict the separation of the jet from the wall. Consequently, the relevant flow patterns (data not shown) obtained using this model on the symmetry plane show only one recirculating area formed by the primary jet.

Overall, the poor predictions given by the $k-\varepsilon$ model can be explained by the overly diffusive character of this model. In addition, according to Wilcox (1994), Menter (1997), the $k-\varepsilon$ model predicted significantly high shear-stress levels and hence delays or completely prevents separation. According to Launder et al. (1975), this trend can be more pronounced in the presence of adverse pressure gradient and leads to overestimation of the wall shear stress. This implies that the non-separation of the jet from the ceiling leads to an intensification of the primary recirculation in

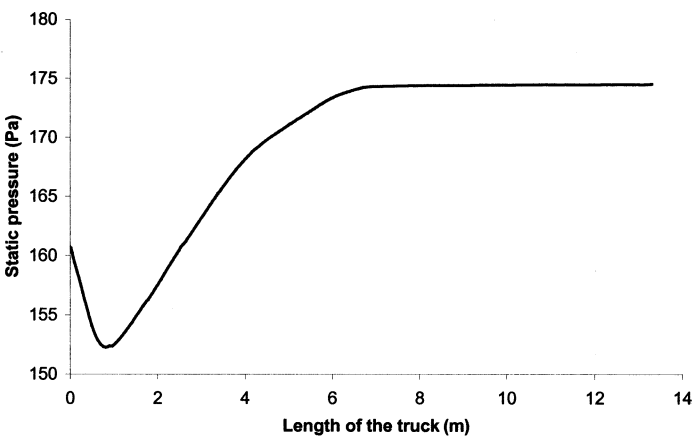


Fig. 5. Evolution of static pressure through middle of flow in a loaded configuration.

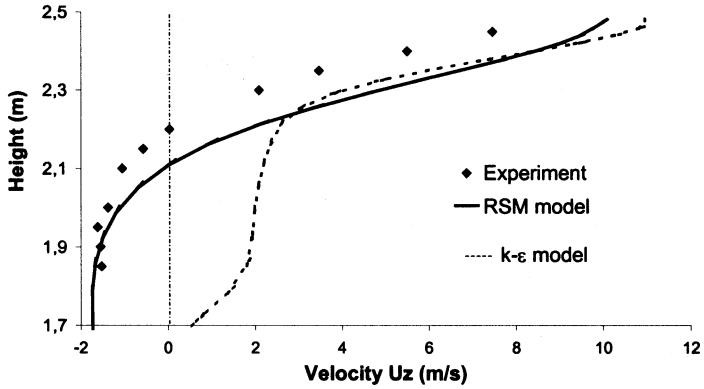


a) 1m

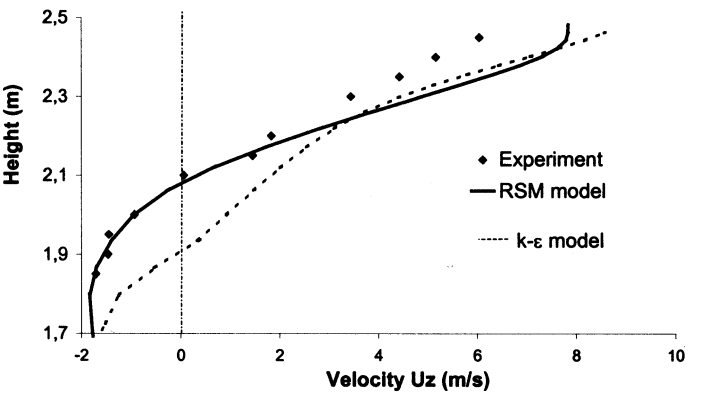


b) 2m

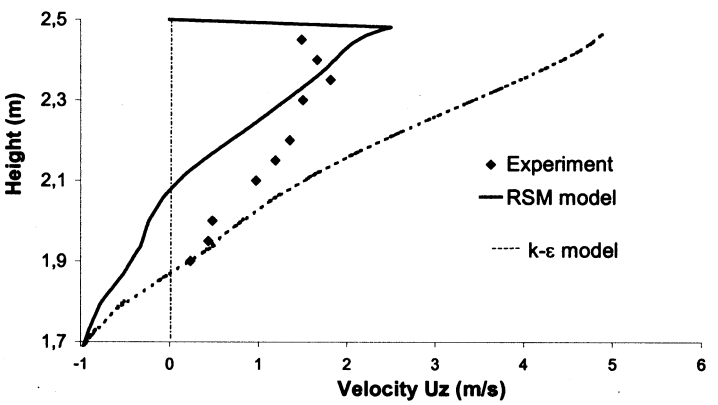


c) 4m

Fig. 6. Vertical profiles of the $U_z$ velocity (a) 1 m (b) 2 m (c) 4 m.

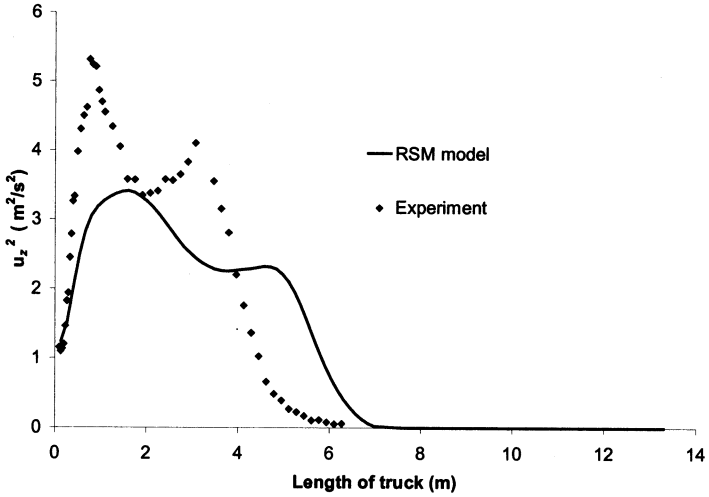


Fig. 7. Evolution of the mean-square of the turbulent velocity in the $z$ direction ($\overline{u_z^2}$).

the whole enclosure. This failure of the $k-\varepsilon$ model to predict complex flows, including secondary and/or separated flows caused by adverse pressure gradient, has been observed by many researchers previously (Wilcox, 1994; Menter, 1997; Nallasamy, 1987).

Fig. 6 shows comparisons between experimental and numerical data obtained by RSM and $k-\varepsilon$ models showing vertical profiles of horizontal velocities ($U_z$) at 1, 2 and 4 m in the medium plane. It can be seen that the RSM model performs better than the $k-\varepsilon$ model for the diffusion of the jet and the location of the center of the recirculation ($U_z = 0$).

### 5.3. Turbulence behavior

Fig. 7 shows comparisons between numerical and experimental data concerning the evolution of the mean-square of the turbulent velocity in the $z$ direction ($\overline{u_z^2}$) through the inlet section along the enclosure in a loaded configuration. Both curves have two peaks. The first peak is a common characteristic of turbulent jet expansion due to diffusion of the turbulence from the edge to the core of the jet. The second peak located near the separation area of the jet from the wall reflects the extra amount of turbulence generated in this region where high gradients of velocities were locally present. Even if the trend of numerical and experimental values are similar, the RSM model seemed to overestimate the diffusive character of the turbulence. Consequently, predicted peak values of $\overline{u_z^2}$ were obviously lower than experimental data.

### 5.4. Aerodynamic behavior of the two recirculating areas

So as to better illustrate the airflow characteristics of each recirculating area, Fig. 8 represents (from numerical data given by the RSM model) the longitudinal evolution along the enclosure of the airflow rate scaled to the inlet flow rate ($Q(z)/Q_0$). For a given cross-section along the enclosure, the circulating flow rate $Q(z)$ was calculated as follows:

$$Q(z) = 0.5 \int_{S_{(z)}} |U_z| \mathrm{d}s \tag{7}$$

where $S_{(z)}$ represents the considered cross-section at $z$ coordinate and $U_z$ represents the local longitudinal velocity normal to $S_{(z)}$.

The results show a clear net aerodynamic contrast between the two recirculating areas. The higher values of flow rate related to the primary recirculation reflect, respectively, the importance of convective and diffusive mechanisms in this area compared with the secondary recirculating area. It can be seen that the flow rate of the primary recirculation was 50% higher than the inlet flow rate and ten times higher than the second recirculating flow rate. Consequently, the air changes per hour used by many researchers (Bennahmias and Labonne, 1993; Meffert and Van Nieuwenhuizen, 1973; Billiard et al., 1990) and defined as the ratio of the inlet flow rate to the useful volume of the truck should be revised and adjusted locally as a function of the behavior of airflow patterns and the evolution of the airflow circulation through the vehicle.

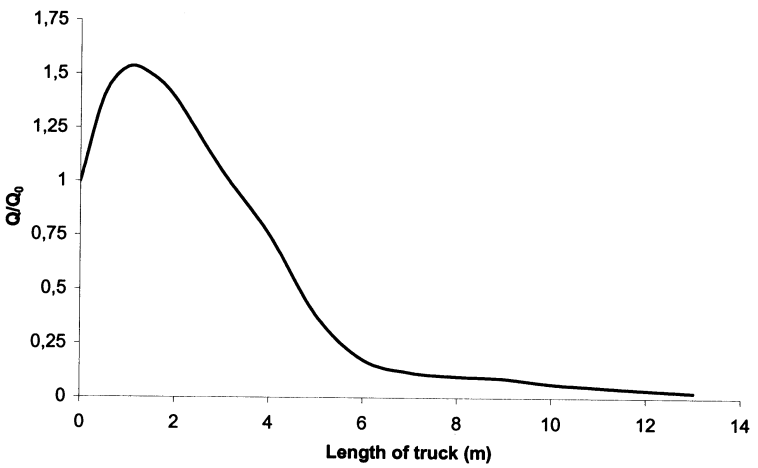


Fig. 8. Evolution of the airflow rate scaled by the inlet flow through the vehicle.

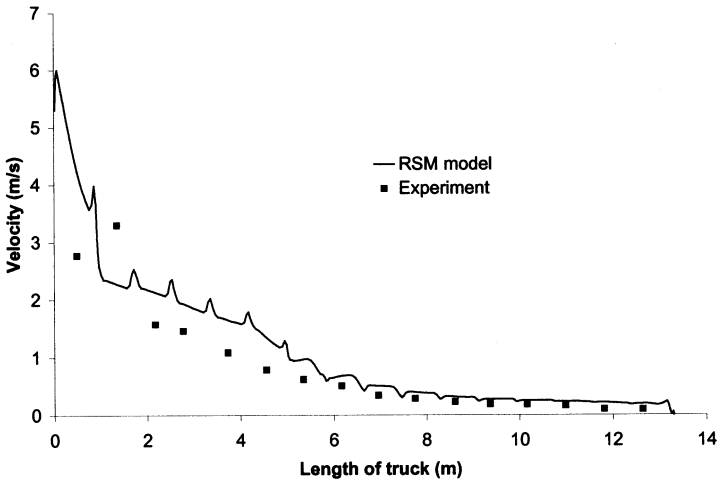


Fig. 9. Evolution of air velocity magnitude between the two rows of pallets.

### 5.5. Secondary flow

In addition to the turbulent zones generated by the jet diffusion, it was also important to investigate secondary flows which were dominated by the inertia phenomena. These zones concern essentially thin air spaces located between wall and pallets (1–2 cm) and between two rows of pallets.

Figs. 9 and 10 present comparisons between experimental and predicted values of air velocities at medium level between wall and pallets and between the two rows of pallets. These figures show clearly that in these spaces the air velocity magnitudes were governed by the behavior of the air wall jets and the presence of primary and secondary recirculations. Consequently, very low velocities were reported and predicted in the rear part of the vehicle just after the separation of the jet from the wall.

As regards the low velocities between the wall and the pallets, heat fluxes exchanged through the insulated wall with the surrounding atmosphere are difficult to remove in this space and high temperatures are expected locally.

## 6. Conclusions

In this study, experiments and numerical simulations performed using the CFD code Fluent were carried out in order to characterize velocities and airflow patterns within a typical RVE loaded with two rows of pallets.

The experiments carried out on a reduced-scale model with Laser–Doppler velocimetry showed the separation of the jet from the wall at approximately 10 m from the inlet in the case of an empty enclosure and 6 m for a loaded configuration.

In order to reduce the cell size and make it possible to use a numerical approach, an original formulation based on an analogy between the porous medium and the laminar flow which was dominant between pallets was used in the numerical model. These simulations clearly showed the ability of the RSM model to accurately predict the separation of the jet from the wall and the general behavior of air movement related to the primary and to the second recirculations in loaded and unloaded configurations. Good agreement between the RSM and experimental data also found for highly turbulent zones generated by the wall jet diffusion as well as low turbulent zones in thin air spaces located inside the load. Conversely, the standard $k-\varepsilon$ model overestimates the diffusive character of the wall jet and fails to accurately predict the separation of the jet from the wall in loaded and unloaded configurations.

This model should be used to improve and to optimize systems of air distribution in refrigerated vehicles and hence to decrease the temperature differences throughout the palletized cargos. This condition is essential in order to preserve the quality, safety and shelf life of perishable products.

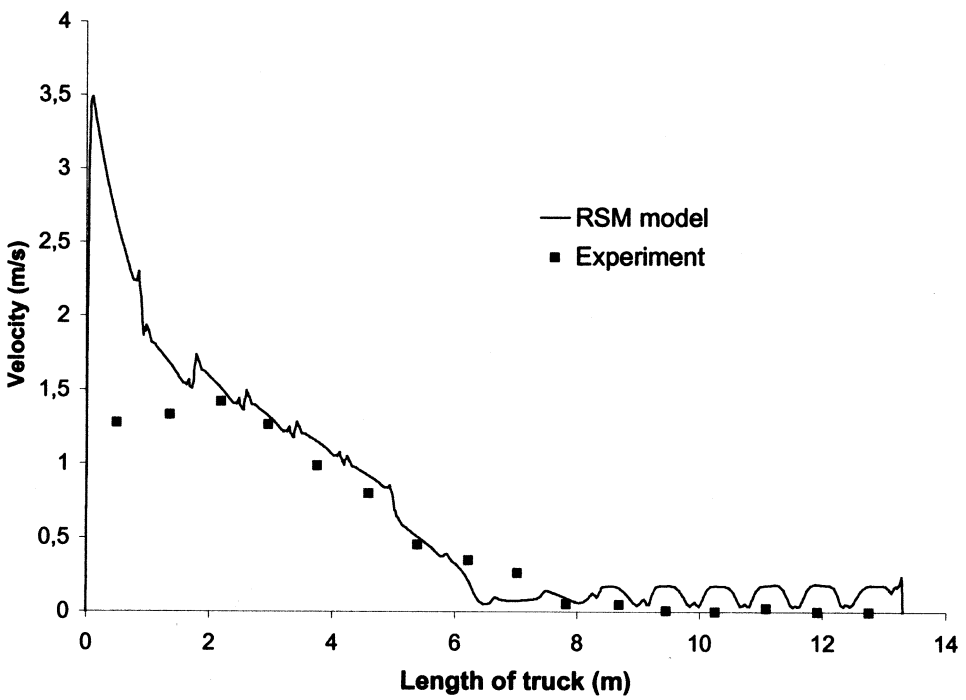


Fig. 10. Evolution of air velocity magnitude between lateral wall and pallets on the medium level.

## References


Awbi, H.B., 1989. Application of computational fluid dynamics in room ventilation. Building Environment 24 (1), 73–84.

Bennahmias, R., Labonne, G., 1993. Etude de la distribution de l'air et de la dispersion des températures dans une semi-remorque. In: Proceedings I.I.F.-I.I.R., Morocco, pp. 241–256.

Billiard, F., Bennahmias, R., Nol, P., 1990. Nouveaux développements dans les transports à température dirigée routiers. In: Proceedings I.I.F.-I.I.R. Commissions B2, C2, D1, D2/3, Dresden, Germany, pp. 793–802.

Chen, Q., 1995. Comparison of different k–ε models for indoor air flow computations. Numerical Heat Transfer, Part B 28, 353–369.

Choi, H.L., Albright, L.D., Timmons, M.B., 1990. An application of the $k$–$\varepsilon$ turbulence model to predict how a rectangular obstacle in a slot-ventilated enclosure affects air flow. Transactions in Agriculture 33 (1), 274–281.

Davidson, L., 1989. Ventilation by Displacement in a Three-Dimensional Room: A numerical study. Building and Environment 24 (4), 263–272.

Gögus, A.Y., Yavuzkurt, S., 1974. Temperature pull-down and distribution in refrigerated trailers. In: Proceedings I.I.F.-I.I.R. Commission D2, Wageningen, pp. 189–193.

Hoang, M.L., Verboven, P., De Baermaeker, J., Nicolaï, B.M., 2000. Analysis of air flow in a cold store by means of computational fluid dynamics. International Journal of Refrigeration 23, 127–140.

Hoff, S.J., Janni, K.A., Jacobson, L.D., 1992. Three-dimensional buoyant turbulent flows in a scaled model, slot-ventilated, livestock confinement facility. Transactions of American Society of Agriculture Engineering 35 (2), 671–686.

Launder, B.E., Spalding, D.B., 1974. The numerical computation of turbulent flows. Computers Methods in Applied Mechanics and Energy 3, 269–289.

Launder, B.E., Reece, G.J., Rodi, W., 1975. Progress in the development of a Reynolds stress turbulence closure. Journal of Fluid Mechanics 68, 537–566.

LeBlanc, D., Beaulieu, C., Lawrence, R., Stark, R., 1994. Evaluation of temperature variation of frozen foods during tranportation. The Refrigeration Research Foundation Information Bulletin, Bethesda, MD, USA.

Lenker, D.H., Woodruff, D.W., Kindya, W.G., Carson, E.A., Kasmire, R.F., Hinsch, R.T., 1985. Design criteria for the air distribution systems of refrigerated vans. Transactions of American Society of Agriculture Engineering 28 (6), 2089–2097.

Lindqvist, R., 1998. Reefer hold air distribution. In: Proceedings I.I.F.-I.I.R. Commissions D1, D2/3, Cambridge, UK.

Lindqvist, R., 1999. Air distribution design for controlled atmosphere in reefer cargo holds. In: Twentieth International Congress of Refrigeration, I.I.F.-I.I.R., Sydney.

Meffert, H.F.T., Van Nieuwenhuizen, G., 1973. Temperature distribution in refrigerated vehicles. In: Proceedings I.I.F.-I.I.R. Commissions D1, D2 and D3, Barcelona, Spain, pp. 131–135.

Meffert, H.F.T., Van Beek, G., 1983. Basic elements of a physical refrigerated vehicles, air circulation and distribution. In: Sixteenth International Congress of Refrigeration, I.I.F.-I.I.R., Paris, pp. 466–475.

Ménia, N.Z., Moureh, J., Flick, D., 2002. Modélisation simplifiée des écoulements d'air dans un véhicule frigorifique. International Journal of Refrigeration, in press.

Menter, F.R., 1997. Eddy viscosity transport equations and their relation to the $k$–$\varepsilon$ model. ASME Journal of Fluids Engineering 119, 876–884.

Nallasamy, M., 1987. Turbulence models and their applications to the prediction of internal flows: a review. Computers and Fluids 15 (2), 151–194.

Nielsen, P.V., Restivo, A., Whitelaw, J.H., 1978. The Velocity Characteristics of Ventilated Rooms. Journal of Fluids Engineering 100, 291–298.

Van Gerwen, R.J.M., Van Oort, H., 1989. Optimization of cold store using fluid dynamics models. In: Proceedings I.I.F.-I.I.R. Commissions B2, C2, D1, D2/3, Dresden, Germany.

Wang, H., Touber, S., 1988. Simple non-steady state modelling of a refrigerated room accounting for air flow and temperature distributions. In: Proceedings I.I.F.-I.I.R. Commissions B1, B2, C2, D1, D2/3, Wageningen, pp. 211–219.

Wang, H., Touber, S., 1990. Distributed dynamic modelling of a refrigerated room. International Journal of Refrigeration 13, 214–222.

Wilcox, D.C., 1994. Turbulence modeling for C.F.D. DCW Industries Inc., La cañada, CA.